Monthly Notices of the ROYAL ASTRONOMICAL SOCIETY

MNRAS **523,** 2641–2650 (2023)
Advance Access publication 2023 May 27

https://doi.org/10.1093/mnras/stad1560

The value-added catalogue of ASAS-SN eclipsing binaries – III. Masses and radii of *Gaia* spectroscopic binaries

D. M. Rowan [1,2]★ T. Jayasinghe,[1,2,3]† K. Z. Stanek,[1,2] C. S. Kochanek,[1,2] Todd A. Thompson [1,2,4] B. J. Shappee[5] and W. Giles[6]

[1]*Department of Astronomy, The Ohio State University, 140 West 18th Avenue, Columbus, OH 43210, USA*
[2]*Center for Cosmology and Astroparticle Physics, The Ohio State University, 191 W. Woodruff Avenue, Columbus, OH 43210, USA*
[3]*Department of Astronomy, University of California Berkeley, Berkeley, CA 94720, USA*
[4]*Department of Physics, The Ohio State University, Columbus, OH 43210, USA*
[5]*Institute for Astronomy, University of Hawaii, 2680 Woodlawn Drive, Honolulu, HI 96822, USA*
[6]*ASC Technology Services, 433 Mendenhall Laboratory, 125 South Oval Mall, Columbus, OH 43210, USA*

Accepted 2023 May 16. Received 2023 April 17; in original form 2022 December 5

ABSTRACT

Masses and radii of stars can be derived by combining eclipsing binary light curves with spectroscopic orbits. In our previous work, we modelled the All-Sky Automated Survey for Supernovae (ASAS-SN) light curves of more than 30 000 detached eclipsing binaries using PHOEBE. Here, we combine our results with 128 double-lined spectroscopic orbits from *Gaia* Data Release 3. We also visually inspect ASAS-SN light curves of the *Gaia* double-lined spectroscopic binaries on the lower main sequence and the giant branch, adding 11 binaries to our sample. We find that only 50 per cent of systems have *Gaia* periods and eccentricities consistent with the ASAS-SN values. We use EMCEE and PHOEBE to determine masses and radii for a total of 122 stars with median fractional uncertainties of 7.9 per cent and 6.3 per cent, respectively.

Key words: surveys – binaries: eclipsing.

1 INTRODUCTION

Accurate measurements of stellar masses and radii are crucial tests for models of stellar structure and evolution. Stellar models contain empirical prescriptions for effects like mass-loss, convective overshoot, mixing, and rotation that alter the stellar properties and need to be accurately calibrated. This needs to be done for stars of different masses, evolutionary states, and metallicities (Andersen 1991).

The measured masses and radii of binary stars are also benchmarks for asteroseismology. Solar-like oscillations can be interpreted using scaling relations to measure stellar masses and radii (Kjeldsen & Bedding 1995). These relations are particularly useful for measuring the masses of red giants, since these stars are not well separated by mass on a colour–magnitude diagram, making mass inference from isochrone fitting challenging. Hekker et al. (2010) identified oscillations in an eclipsing red giant using Kepler photometry. Dynamical masses and radii were derived from spectroscopic follow-up (Frandsen et al. 2013) and were found to be in agreement with the asteroseismic masses and radii, supporting the scaling relations (Themeßl et al. 2018). Since then, a number of authors have used *Kepler* and *Transiting Exoplanet Survey Satellite* (*TESS*) photometry to identify oscillating giants in eclipsing binaries (Gaulme et al. 2013; Beck et al. 2014; Gaulme et al. 2014; Brogaard et al. 2018; Benbakoura et al. 2021; Beck et al. 2022), and these systems suggest that radii are overestimated by ~ 5 per cent and masses are overestimated by ~ 15 per cent when using asteroseismic scaling relations (Gaulme et al. 2016).

Accurate stellar parameters are also needed to characterize exoplanets, since most of the observed properties of transiting exoplanets are measured relative to that of their host star (Eastman, Gaudi & Agol 2013; Rodríguez Martínez et al. 2023). Theoretical evolutionary tracks or empirical relations derived from eclipsing binaries can be used, but this assumes that the star is typical in terms of mass, metallicity, and rotation rate within the sample of stars used to derive these relations (Enoch et al. 2010; Torres, Andersen & Giménez 2010; Duck et al. 2022).

Masses and radii of stars can be determined by starting from catalogues of eclipsing binaries found by photometric surveys such as the Optical Gravitational Lensing Experiment (Graczyk et al. 2011; Pawlak et al. 2013; Pietrukowicz et al. 2013; Soszyński et al. 2016; Bódi & Hajdu 2021), *Kepler* (Prša et al. 2011; Slawson et al. 2011; Kirk et al. 2016), the Wide-field Infrared Survey Explorer (Petrosky et al. 2021), the All-Sky Automated Survey (ASAS; Pojmanski 2002; Paczyński et al. 2006), and *TESS* (Ricker et al. 2015; Prša et al. 2022). Physical masses and radii can be determined by combining the eclipsing binary light curve with radial velocity observations (e.g. Hełminiak et al. 2021; Ratajczak et al. 2021).

Large spectroscopic surveys such as the Apache Point Observatory Galactic Evolution Experiment (Majewski et al. 2017), the Large Sky Area Multi-Object Fiber Spectroscopic Telescope (LAMOST; Cui et al. 2012), and the Radial Velocity Experiment (Steinmetz et al. 2006) can also be combined with photometric surveys to constrain stellar parameters. Even for systems with few radial velocity epochs,

★ E-mail: rowan.90@osu.edu
† NASA Hubble Fellow.

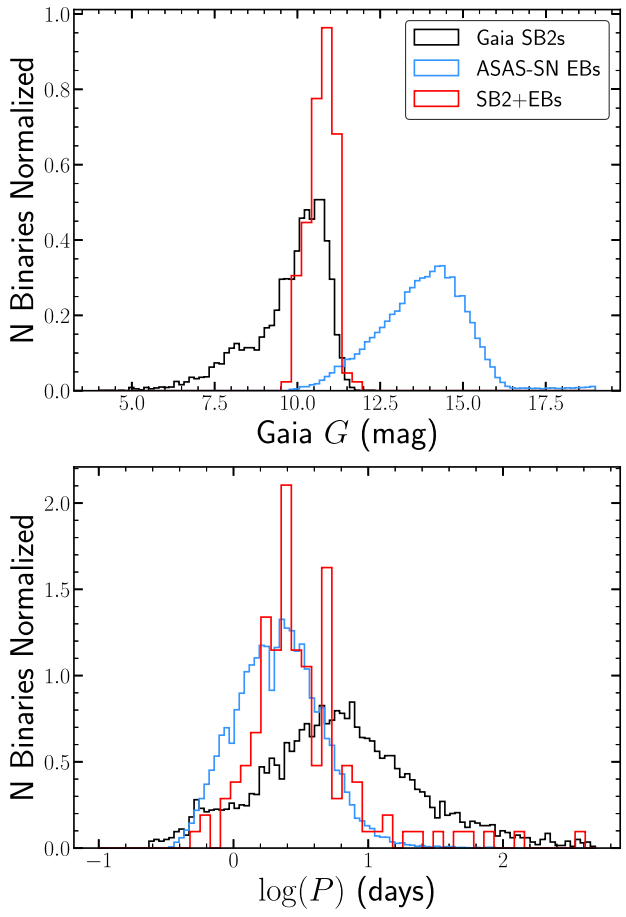

Figure 1. Top: normalized distributions of *Gaia* apparent *G*-band magnitudes for *Gaia* SB2s, ASAS-SN eclipsing binaries, and the cross-matched systems. Bottom: distribution of orbital periods. The *Gaia* spectroscopic binaries extend to longer orbital periods since the detectability of eclipsing binaries drops off as $P^{-2/3}$.

an eclipsing binary light curve can provide the precise period and ephemeris, so stellar and orbital parameters can often be determined (e.g. Qian et al. 2017, 2018; Hambleton et al. 2022). However, only fractions of these catalogues contain the double-lined spectroscopic binary orbits necessary to derive stellar masses and radii (e.g. Kounkel et al. 2021).

Gaia DR3 has significantly expanded the quantity of available spectroscopic data. Nearly 1 million stars have mean RVS spectra (Gaia Collaboration 2022). Although individual epoch radial velocities are only available for <2000 RR Lyrae and Cepheid stars, *Gaia* DR3 includes spectroscopic orbit parameters for more than 181 000 single-lined spectroscopic binaries (SB1s) and more than 5000 double-lined spectroscopic binaries (SB2s) with $G < 12$ mag.

In Rowan et al. (2022, hereafter R22), we modelled the light curves of more than 30 000 detached eclipsing binaries from the All-Sky Automated Survey for Supernovae (ASAS-SN; Shappee et al. 2014; Kochanek et al. 2017; Jayasinghe et al. 2019). We used PHOEBE (Prša & Zwitter 2005; Prša et al. 2016; Conroy et al. 2020) to fit the *V*- and *g*-band light curves, producing a catalogue of orbital periods, eccentricities, inclinations, effective temperature ratios, and sum of the radii relative to the semimajor axis. By combining our catalogue with colours and magnitudes from *Gaia*, three-dimensional dust maps of the Milky Way from `mwdust` (Drimmel, Cabrera-Lavers & López-Corredoira 2003; Marshall et al. 2006; Bovy et al. 2016; Green et al. 2019), and MIST isochrones and evolutionary tracks (Choi et al. 2016; Dotter 2016), we examined the properties of the systems as a function of their absolute magnitude and evolutionary state. In Rowan et al. (2023), we characterized the properties of more than 700 binaries with spots, pulsations, and triple/quadruple systems using ASAS-SN and *TESS* (Ricker et al. 2015; Huang et al. 2020a,b; Kunimoto et al. 2021).

Here, we combine the R22 'value-added' catalogue of eclipsing binaries with the SB2 orbit solutions from *Gaia* DR3. In Section 2, we cross-match the value-added catalogue with the catalogue of *Gaia* SB2s. We also visually inspect ASAS-SN light curves for SB2s in sparsely populated areas of the colour–magnitude diagram (CMD) to identify more eclipsing SB2s. We then compare the *Gaia* and ASAS-SN orbital periods and eccentricities to identify systems with reliable *Gaia* orbital solutions. In Section 3, we use PHOEBE to model the light curve of the detached eclipsing binary with the orbital constraints from *Gaia*. Finally, we present the distribution of stellar parameters in Section 4.

2 ECLIPSING BINARIES WITH SPECTROSCOPIC ORBITS

Gaia DR3 includes a total of 5376 systems with SB2 orbit solutions in the `nss_two_body_orbit` table. The majority of the targets are fairly bright, with apparent *G* magnitudes ranging from 3.6 to 12.2 mag and a median of 10.1 mag. 1053 of the *Gaia* SB2s are labelled as photometrically variable in *Gaia* DR3 and 533 are included in the `vari_eclipsing_binary` table. The optimal magnitude range for ASAS-SN targets is 11 mag $< V <$ 17 mag and 12 mag $< g <$ 18 mag. Fig. 1 shows the distribution of apparent *G* magnitude for the *Gaia* SB2 catalogue and the value-added EB catalogue.

We start by performing a positional cross-match with a search radius of 5 arcsec and identify 128 targets in common between the SB2 and EB catalogues. Fig. 1 shows that these targets are found in the bright tail of the ASAS-SN catalogue and the faint end of the SB2 catalogue. The bottom panel of Fig. 1 shows that the majority of systems identified in the cross-match have orbital periods $P < 10$ d, although there are a handful of long-period systems included in both catalogues. The orbital period of the 128 targets ranges from 0.62 to 124.9 d with a median value of 2.68 d.

We use distances from Bailer-Jones et al. (2021), which include colour and magnitude priors as part of the distance estimate, and extinction estimates from the `mwdust` (Bovy et al. 2016) three-dimensional 'Combined19' dust map (Drimmel et al. 2003; Marshall et al. 2006; Green et al. 2019) to determine the extinction-corrected absolute magnitude and colour. We use the MESA Isochrones & Stellar Tracks (MIST; Choi et al. 2016; Dotter 2016) and follow the procedure described in R22 to divide the CMD into systems with main sequence, subgiant, and giant primaries. To remove systems with poor parallax or extinction estimates, we only report the evolutionary state for systems where the parallax divided by its standard error is `parallax_over_error` > 10 and $A_V < 2.0$ mag. These values are chosen to be consistent with R22. Fig. 2 shows the distribution of the SB2 catalogue, the EB catalogue, and the cross-match between them on the CMD. For stars with $M_G \lesssim 4$ mag, there are fewer SB2s than ASAS-SN EBs below the binary main sequence since systems of nearly equal mass are more easily characterized in SB2 analysis.

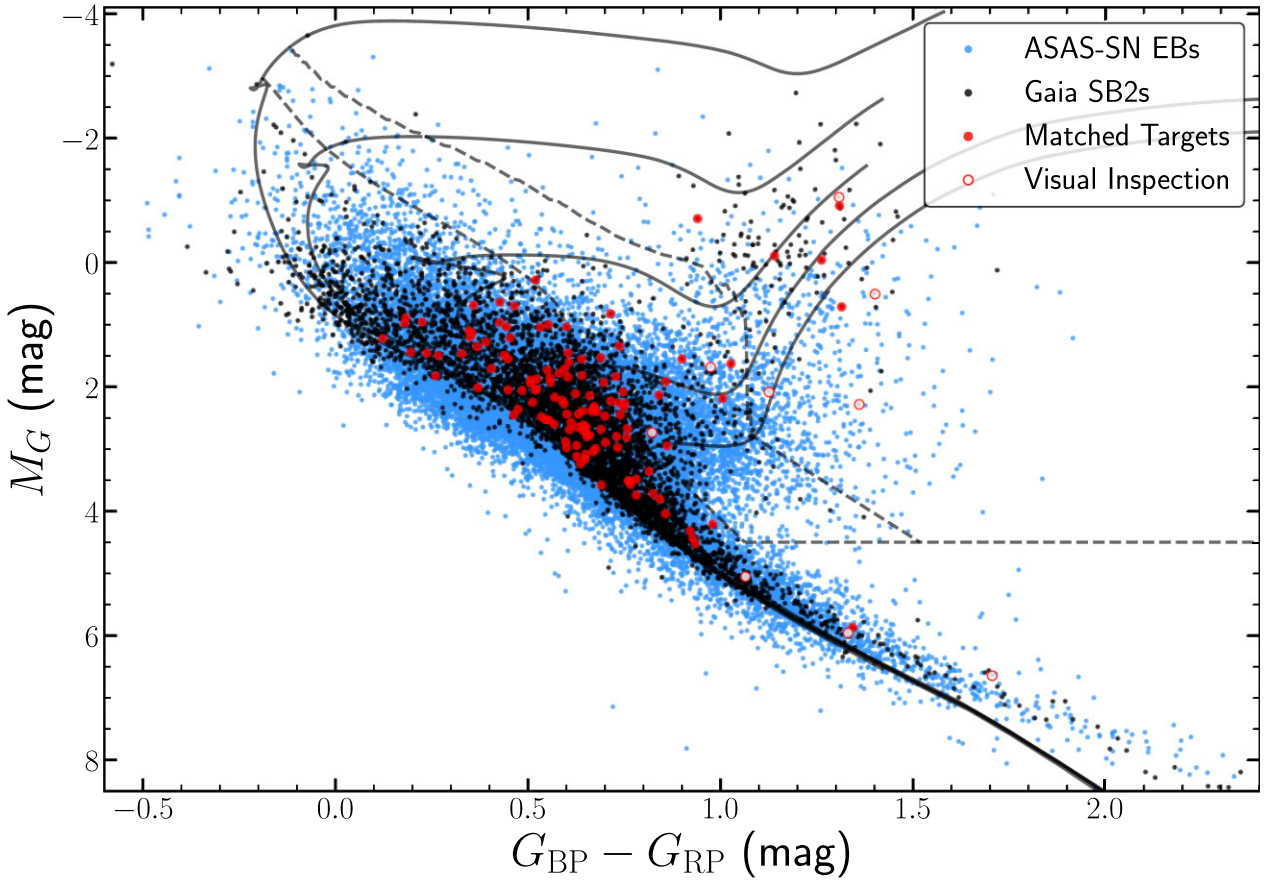

Figure 2. The extinction-corrected *Gaia* DR3 colour–magnitude diagram (CMD). The ASAS-SN detached eclipsing binaries from R22 are shown in blue, the 5376 *Gaia* SB2s are shown in black, and the eclipsing spectroscopic binaries are shown in red. The solid lines show MIST isochrones for ages of 10^8–10^{10} yr in intervals of 0.5 dex. The flux of the isochrones is doubled in each band to represent binary stars of equal mass. The dashed lines show the boundaries of the giant and subgiant branches defined by R22. We note that one binary in the visual inspection group, CM Dra (*Gaia* DR3 1431176943768690816) is at $M_G \sim$ 10.6 mag, below the range of this figure.

The majority of the SB2 + EB binaries are on the main sequence, although 18 and 5 are found on the subgiant and giant branch, respectively. We used ASAS-SN Sky Patrol v2 (Hart et al. 2023) to visually inspect the *g*-band light curves of all 5376 systems in the *Gaia* SB2 catalogue folded at the *Gaia* orbital period. In total, we identify 200 additional eclipsing binaries, but many are saturated in ASAS-SN ($V \lesssim 10$). To expand our sample to stars of a wider range of mass and evolutionary state, we focus on either end of the main sequence ($M_G < 1$ mag or $M_G > 5$ mag) and stars that are subgiants/giants based on the CMD position and MIST isochrones. Fig. 2 shows the 11 targets we added to our EB + SB2 catalogue to expand our coverage of the CMD. While we add additional low-mass main-sequence and giant/subgiant binaries, the early-type binaries that we identified during visual inspection all have saturated ASAS-SN light curves.

Although we expect the *Gaia* orbital period to be correct for these 11 systems since we identified the eclipses in the phase-folded light curve, we start by running the `astrobase` implementation of box least squares (BLS) periodogram (Kovács, Zucker & Mazeh 2002; Bhatti, lgbouma & Joshua 2018) to determine a more precise period. We use a narrow period search window of ±20 per cent of the *Gaia* orbital period. We manually clip outlying points due to saturation effects in the light curves. We then follow the procedure described in R22 to estimate the orbital inclination, eccentricity, argument of periastron, the ratio of effective temperatures, and the sum of the fractional radii with PHOEBE (Prša & Zwitter 2005; Prša et al. 2016; Conroy et al. 2020). To summarize the procedure, we start by combining the results from the PHOEBE geometry estimator (Mowlavi et al. 2017) and the 'eclipsing binaries via artificial intelligence' estimator (Prša et al. 2008) as initial estimations for the Nelder–Mead optimizer (Gao & Han 2012). The resulting model will be used to set the initial conditions for the Markov chain Monte Carlo (MCMC) fits.

Before we adopt values of the velocity semi-amplitudes from the *Gaia* SB2 solutions, we compare the ASAS-SN and *Gaia* periods and eccentricities to identify and remove poor SB2 orbital solutions. Fig. 3 shows the ASAS-SN and *Gaia* orbital periods and eccentricities. We consider the SB2 solution to be reliable if the *Gaia* orbital period is within 10 per cent of the ASAS-SN orbital period. We also require the *Gaia* eccentricity to be within 25 per cent of the ASAS-SN eccentricity, or both eccentricities to be $e < 0.05$. In total, only 70 SB2 + EB systems meet these quality cuts. 18 of the systems with discrepant *Gaia* periods are relatively faint ($G \gtrsim 11$ mag), which could suggest lower-quality *Gaia* SB2 orbital fits in the tail of the magnitude distribution. This magnitude dependence is less clear for the comparison of eccentricities, but some of the systems where the ASAS-SN light curve suggests a near-circular orbit ($e \lesssim 0.01$) and *Gaia* prefers an eccentric orbit are also faint.

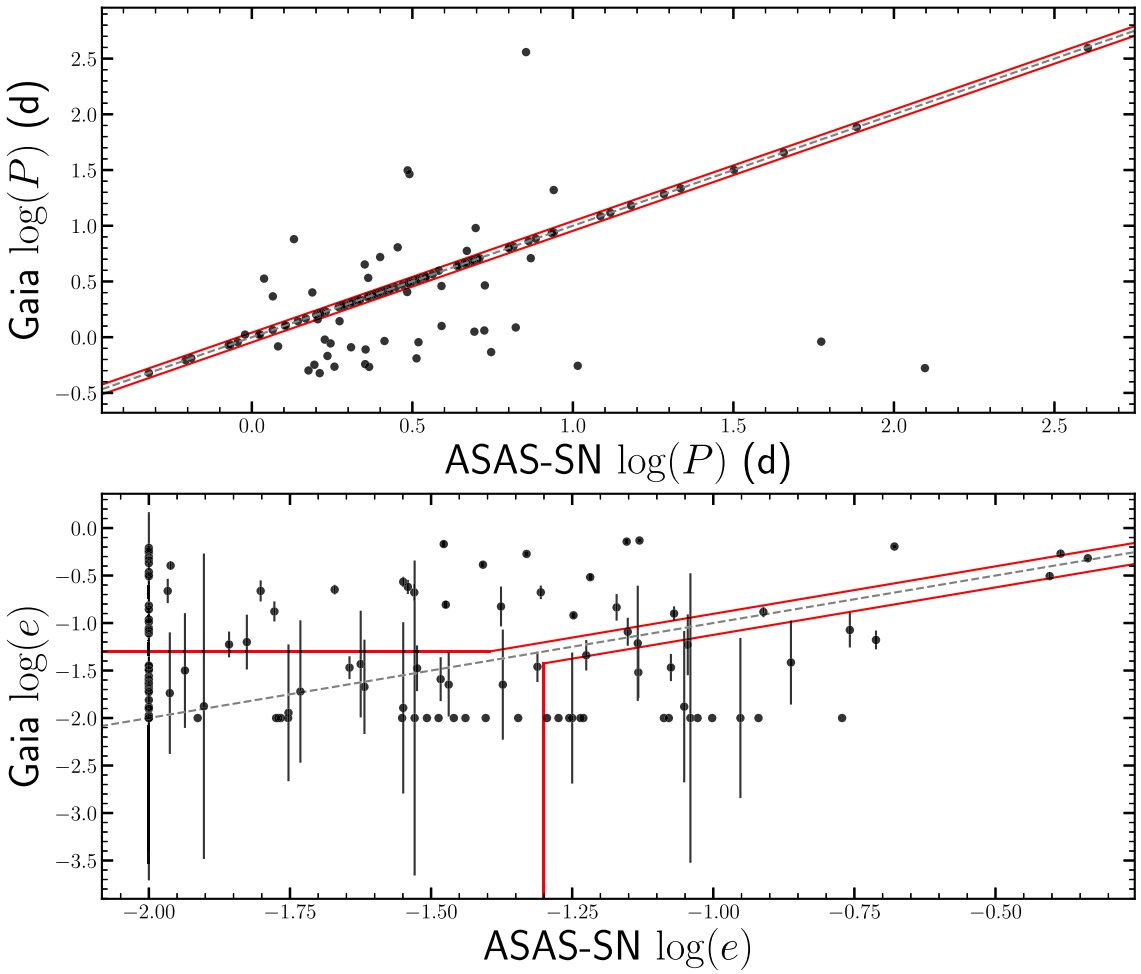

Figure 3. Comparison of periods and eccentricities from the *Gaia* SB2 orbits and ASAS-SN eclipsing binary light curves. The grey lines show the expected equality between the ASAS-SN and *Gaia* values. The region in between the red lines shows where we define the periods and eccentricities to be consistent. Eccentricities $\log e < -2$ are shown as $\log e = -2$ for this figure.

While it may seem surprising that only ~ 50 per cent of *Gaia* SB2s have reliable orbits in our sample, similar disagreements have been found between *Gaia* SB1s and external catalogues. Jayasinghe et al. (2023) compared the *Gaia* SB1s to the Ninth Catalog of Spectroscopic Orbits (SB9; Pourbaix et al. 2004) and found only ~ 80 per cent (~ 70 per cent) of the *Gaia* solutions had periods (eccentricities) matching the SB9 results. Similarly, Bashi et al. (2022) used LAMOST and GALAH radial velocities to consider which SB1s may have incorrect orbital parameters and found that many of the short-period *Gaia* SB1s have erroneously high eccentricities.

Fig. 4 shows the distribution of the *Gaia* `goodness_of_fit` and significance parameters. The `goodness_of_fit` reports the 'Gaussianized Chi-Square' statistic and is expected to have a median of zero and standard deviation of one, although we note that the median value for the full SB2 sample is 10.92. The top panel of Fig. 4 shows that the SB2s with periods and eccentricities matching the ASAS-SN light-curve solution generally have lower `goodness_of_fit` values. However, the systems with poor *Gaia* orbital fits are found from $-1 \leq$ `goodness_of_fit` < 40, and there is no cut-off in `goodness_of_fit` that could be used to select for reliable SB2 solutions. The significance parameter is defined as the ratio between the velocity semi-amplitude of the primary and its uncertainty, K_1/σ_{K_1}. While this statistic is generally useful for rejecting poor (significance $\lesssim 20$) solutions (e.g. Bashi et al. 2022; Jayasinghe et al. 2023), there is also no significance cut-off that can be used to reject unreliable *Gaia* SB2 orbital solutions. Bashi et al. (2022) combined the SB1 period, semi-amplitude, number of observations, goodness of fit, RV amplitude, and RV signal-to-noise ratio parameters to construct a 'Score' statistic, but some of these parameters are not available for the *Gaia* SB2 sources. Since *Gaia* DR3 only provides the spectroscopic orbital solutions and not the individual radial velocities, it is clearly important to be cautious when interpreting the ensemble statistics in the *Gaia* `nss_two_body_orbit` SB2 tables given that only 50 per cent of our eclipsing SB2s have reliable *Gaia* periods and eccentricities.

3 ECLIPSING BINARY MODEL FITTING

For the 70 systems where the period and eccentricity of the *Gaia* SB2 solution are consistent with the results of the eclipsing binary model fit, we use PHOEBE to derive the stellar parameters. PHOEBE, and similar tools such as ELC (Orosz & Hauschildt 2000), model the distorted surfaces of binary stars to produce or model the light curves and RV curves of EBs. In R22, we used PHOEBE to model the light curves using Nelder–Mead optimization. Here, we start

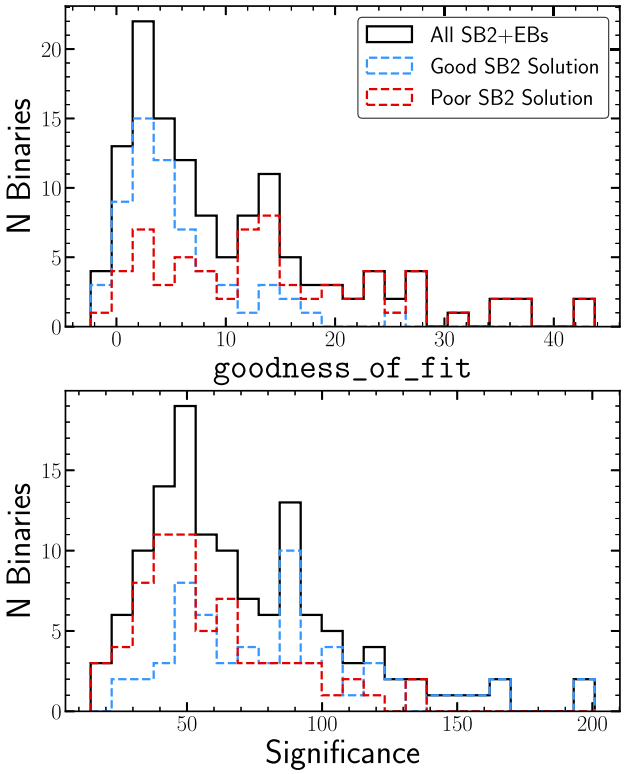

Figure 4. Distributions of the *Gaia* `goodness_of_fit` (top) and significance (bottom) for the full SB2 + EB sample. We identify good orbital fits by comparing the *Gaia* and ASAS-SN periods and eccentricities (Fig. 3).

from our existing PHOEBE model with either the ASAS-SN *V*- or *g*-band light curve, selecting the light curve that is less affected by saturation.

PHOEBE includes multiple modes for relating the flux of the input light curve to the synthetic light curve. In R22, we set this passband luminosity mode to `dataset-scaled` so that the model fluxes are automatically scaled to match the flux-levels of the observations. Here, we change the passband luminosity mode to `component--coupled`, which uses the physical passband luminosity, $L_{\rm pb}$ for one star rather than a scaling based on the normalized fluxes. This will include any correlations between the passband luminosity and other sampled parameters in the MCMC sampling.[1] To set an initial value of $L_{\rm pb}$ before fitting with MCMC, we run 200 iterations of Nelder–Mead optimization with $L_{\rm pb}$, the effective temperature ratio $T_{\rm eff,2}/T_{\rm eff,1}$, and the fractional radii R_1/a and R_2/a, where a is the semimajor axis, as free parameters.

We then set the mass ratio used by PHOEBE to be $q = K_1/K_2$, where K_1 and K_2 are the *Gaia* RV semi-amplitudes. We also set the projected semimajor axis of the secondary to

$$a_2 \sin(i) = K_2 \left(\frac{P}{2\pi}\right) \sqrt{1-e^2}. \quad (1)$$

We use EMCEE (Foreman-Mackey et al. 2013) within PHOEBE to perform an MCMC fit on the ASAS-SN light curve. We set Gaussian priors on q and $a_2 \sin(i)$ using the *Gaia* DR3 values and errors on K_1 and K_2. The orbital period is fixed at the value from the BLS periodogram of the ASAS-SN light curve.

We sample over the mass ratio, q, the primary mass, M_1, the radii R_1 and R_2, the inclination i, the eccentricity, e, and the passband luminosity $L_{\rm pb}$. We found that 5000 MCMC iterations with 35 walkers was sufficient for convergence. We discard the first 1000 iterations as 'burn-in'. For some targets where the walkers have not yet converged by 1000 iterations, we run an additional 2000 iterations, increasing the burn-in accordingly. In some cases, a few ($\lesssim$5) of the walkers fail to converge. We manually set cut-offs in the log-probability of the walkers for these systems before adopting the final posterior distributions. Fig. 5 shows an example of the MCMC posteriors and light-curve fit for *Gaia* DR3 154197232963101568.

We calculate the Roche lobe filling fraction, $f = R/R_{\rm roche}$, where $R_{\rm roche}$ can be estimated from the approximation (Eggleton 1983),

$$R_{\rm roche}/a = \frac{0.49q^{2/3}}{0.6q^{2/3} + \ln\left(1+q^{1/3}\right)}. \quad (2)$$

The filling fraction can be used to evaluate the degree to which systems are detached and can be thought of as evolving independently, without mass transfer.

4 RESULTS

Table 1 reports the *Gaia* Source information, MCMC posteriors, and the evolutionary state of the primary based on its CMD position. All of the light curves and corner plots are available online at https://asas-sn.osu.edu/binaries/mass-radius, and in the electronic version of the paper.

Fig. 6 shows the masses and radii of our sample. The grey dashed line shows the single star solar metallicity zero-age main sequence (ZAMS) from the MIST (Choi et al. 2016; Dotter 2016). Fig. 6 also compares our sample to the masses and radii in Torres et al. (2010). The Torres et al. (2010) catalogue includes the selection criteria that both components have masses and radii errors < 3 per cent, so it is not surprising that our uncertainties on the stellar parameters are larger, but we find results consistent with expectations for main-sequence stars. We report masses and radii of 12 stars on the giant branch, a sparsely populated region in the Torres et al. (2010) catalogue. Our catalogue also has fewer high-mass main sequence stars. This is primarily due to the saturation limit of ASAS-SN, but *Gaia* RVS data also uses the limit $T_{\rm eff} < 14\,500$ K, which is shown by the grey dotted line in Fig. 6 for solar-metallicity evolutionary tracks. We did identify $\sim$10 eclipsing binaries on the upper main sequence during visual inspection, but all had saturated ASAS-SN light curves. The lowest mass system in our catalogue, CM Draconis, was also included in the Torres et al. (2010) catalogue, and our results are consistent within 1σ.

Some of our stars have masses and radii that place them below the ZAMS line. The deviation from the solar metallicity ZAMS is too large to be a metallicity effect, so these stars probably have poor *Gaia* SB2 solutions or histories of mass transfer. Some of these systems are at shorter orbital periods, but only one system (*Gaia* DR3 5380580890642502144) has a component with a large Roche lobe filling fraction (>0.4), suggesting mass transfer may not be the source of the deviation. These systems also do not have large `goodness_of_fit` values.

There are also three stars with $M < 1$ M$_\odot$ and $R > 2$ R$_\odot$. Two of these are in the same binary, *Gaia* DR3 5339144356205089408. This system has Roche lobe filling fractions of $f_1 = 0.48$ and $f_2 = 0.94$ for the primary and secondary, respectively, which may indicate a history of mass transfer. The third star with low mass and large

[1] Additional information about the PHOEBE passband luminosity modes can be found in the PHOEBE documentation: http://phoebe-project.org/docs/latest/tutorials/pblum.

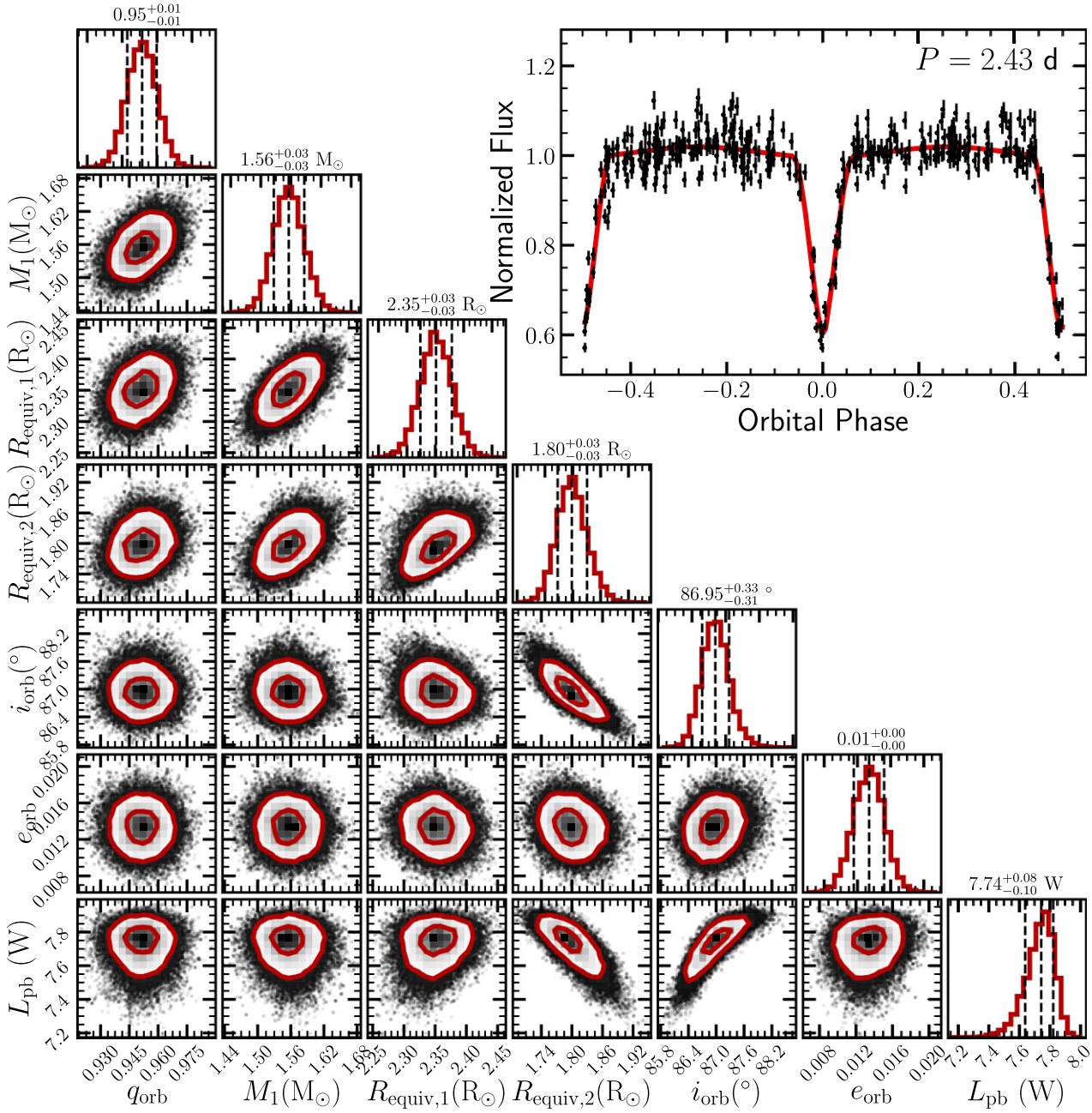

Figure 5. MCMC corner plot and light-curve fit for *Gaia* DR3 154197232963101568.

radius is *Gaia* DR3 1762094209603752192. The other star in this binary is on the subgiant branch, with $M_1 = 2.15$ M$_\odot$ and $R_1 = 4.3$ R$_\odot$. There is also a large difference in eclipse depth (see Fig. 7), suggesting that the more luminous star is also hotter. Both stars have Roche lobe filling factors $0.5 < f < 0.6$, which could suggest that if mass transfer did occur, it is not currently ongoing.

Fig. 8 shows the distribution of the mass and radius uncertainties. For systems with asymmetric posteriors, we report the larger of the $\pm 1\sigma$ uncertainties. The median uncertainty on the mass is 7.9 per cent, and the median uncertainty on the radius is 6.3 per cent. *Gaia* DR3 includes two solution types for SB2s: a standard double-lined binary where the eccentricity is a free parameter (NSSmodel = SB2) and a simplified, circular model (NSSmodel = SB2C). Fig. 8 shows that the binaries with the circular orbit model correspond to almost all of the systems with high fractional errors on the mass and the radius.

The SB2s with the circular orbit model also generally have higher errors on the velocity semi-amplitude of the secondary, σ_{K_2} (Fig. 9). Since the velocity semi-amplitudes are used in our PHOEBE models to set the mass ratio, projected semimajor axis, and the priors for the MCMC runs, a large σ_{K_2} will produce a large σ_M/M. If we only consider binaries with NSSmodel = SB2, the median uncertainty on the mass is 4.8 per cent and the median uncertainty on the radius is 6.3 per cent.

Table 1. Stellar parameters from the MCMC fits to the ASAS-SN light curves with constraints from *Gaia* spectroscopic orbits. The Roche lobe filling fractions of the primary and secondary are f_1 and f_2, respectively. The evolutionary state is based on the CMD position in Fig. 2. The full table is available online at https://asas-sn.osu.edu/binaries/mass-radius and in the electronic version of the paper.

Gaia DR3 source	Period (d)	Mass ratio	M_1 ($M_\odot$)	M_2 ($M_\odot$)	R_1 ($R_\odot$)	R_1 ($R_\odot$)	f_1	f_1	e	i (°)	State
40 041 022 325 608 704	2.808646	$0.99^{+0.03}_{-0.03}$	$1.28^{+0.11}_{-0.10}$	$1.27^{+0.13}_{-0.12}$	$1.47^{+0.11}_{-0.15}$	$1.30^{+0.15}_{-0.15}$	0.338415	0.300173	$0.01^{+0.01}_{-0.01}$	$85.76^{+0.37}_{-0.21}$	MS
154197232963101568	2.431772	$0.95^{+0.01}_{-0.01}$	$1.56^{+0.03}_{-0.03}$	$1.48^{+0.04}_{-0.04}$	$2.35^{+0.03}_{-0.03}$	$1.80^{+0.03}_{-0.03}$	0.556776	0.435488	$0.01^{+0.00}_{-0.00}$	$86.95^{+0.33}_{-0.31}$	SG
428267308105062528	3.289680	$0.95^{+0.21}_{-0.10}$	$1.89^{+0.85}_{-0.63}$	$1.83^{+0.60}_{-0.56}$	$1.95^{+0.27}_{-0.33}$	$1.96^{+0.43}_{-0.33}$	0.354284	0.361245	$0.01^{+0.00}_{-0.00}$	$83.98^{+0.44}_{-0.33}$	MS
453147263375440384	4.586150	$0.98^{+0.02}_{-0.02}$	$1.84^{+0.10}_{-0.09}$	$1.81^{+0.12}_{-0.10}$	$3.03^{+0.10}_{-0.24}$	$2.28^{+0.35}_{-0.24}$	0.445720	0.336974	$0.00^{+0.00}_{-0.00}$	$84.31^{+0.79}_{-0.55}$	MS
533425940213217920	4.860321	$0.97^{+0.02}_{-0.02}$	$1.54^{+0.06}_{-0.06}$	$1.48^{+0.08}_{-0.07}$	$2.63^{+0.07}_{-0.07}$	$2.39^{+0.08}_{-0.07}$	0.394413	0.363752	$0.00^{+0.00}_{-0.00}$	$87.43^{+0.16}_{-0.13}$	SG
535419732749344000	2.948269	$0.87^{+0.32}_{-0.03}$	$2.44^{+0.43}_{-0.37}$	$2.13^{+0.33}_{-0.31}$	$1.91^{+0.12}_{-0.10}$	$4.33^{+0.22}_{-0.22}$	0.340413	0.821817	$0.00^{+0.00}_{-0.00}$	$87.73^{+1.59}_{-2.20}$	SG
555108687465591040	6.334426	$0.95^{+0.14}_{-0.04}$	$1.00^{+0.17}_{-0.14}$	$0.96^{+0.14}_{-0.12}$	$0.91^{+0.11}_{-0.09}$	$0.95^{+0.08}_{-0.10}$	0.131480	0.139853	$0.06^{+0.00}_{-0.00}$	$88.67^{+0.29}_{-0.15}$	MS
583022706417479296	12.185384	$0.96^{+0.01}_{-0.01}$	$1.20^{+0.03}_{-0.03}$	$1.15^{+0.04}_{-0.04}$	$3.93^{+0.52}_{-0.52}$	$3.93^{+0.73}_{-1.27}$	0.347034	0.353851	$0.01^{+0.01}_{-0.01}$	$83.30^{+4.82}_{-1.34}$	SG
681609355666984192	2.703459	$0.96^{+0.14}_{-0.05}$	$1.54^{+0.29}_{-0.26}$	$1.48^{+0.23}_{-0.23}$	$2.52^{+0.17}_{-0.18}$	$1.47^{+0.21}_{-0.16}$	0.559009	0.332373	$0.00^{+0.00}_{-0.00}$	$79.89^{+0.94}_{-0.94}$	MS
690638579515175552	2.380733	$0.96^{+0.01}_{-0.01}$	$1.18^{+0.03}_{-0.03}$	$1.13^{+0.04}_{-0.03}$	$1.62^{+0.21}_{-0.22}$	$1.67^{+0.14}_{-0.24}$	0.428208	0.447758	$0.00^{+0.00}_{-0.00}$	$85.24^{+0.75}_{-0.38}$	MS
690885522954174080	0.647598	$0.81^{+0.04}_{-0.04}$	$0.87^{+0.10}_{-0.10}$	$0.70^{+0.11}_{-0.10}$	$1.05^{+0.04}_{-0.04}$	$0.63^{+0.03}_{-0.03}$	0.721960	0.474742	$0.11^{+0.01}_{-0.01}$	$84.77^{+0.36}_{-0.62}$	MS
947509303493752832	3.481821	$0.99^{+0.05}_{-0.05}$	$1.23^{+0.20}_{-0.17}$	$1.22^{+0.23}_{-0.20}$	$1.31^{+0.10}_{-0.09}$	$1.23^{+0.09}_{-0.09}$	0.263934	0.248808	$0.00^{+0.00}_{-0.00}$	$88.55^{+0.19}_{-0.15}$	MS
1204875013864088576	3.288118	$0.97^{+0.12}_{-0.14}$	$1.64^{+0.72}_{-0.59}$	$1.56^{+0.86}_{-0.63}$	$1.97^{+0.38}_{-0.36}$	$2.89^{+0.85}_{-1.24}$	0.375038	0.561835	$0.01^{+0.01}_{-0.01}$	$72.44^{+4.40}_{-2.17}$	MS
1272930282497618048	5.117104	$0.95^{+0.07}_{-0.08}$	$1.43^{+0.40}_{-0.26}$	$1.34^{+0.44}_{-0.26}$	$2.98^{+0.29}_{-0.30}$	$2.11^{+0.36}_{-0.20}$	0.440978	0.322579	$0.00^{+0.00}_{-0.00}$	$88.73^{+0.85}_{-3.41}$	SG
1387290280744129152	0.846993	$0.76^{+0.62}_{-0.04}$	$1.77^{+0.58}_{-0.49}$	$1.36^{+0.40}_{-0.37}$	$1.28^{+0.12}_{-0.13}$	$1.46^{+0.14}_{-0.15}$	0.577313	0.741876	$0.00^{+0.00}_{-0.00}$	$87.25^{+0.26}_{-0.21}$	MS

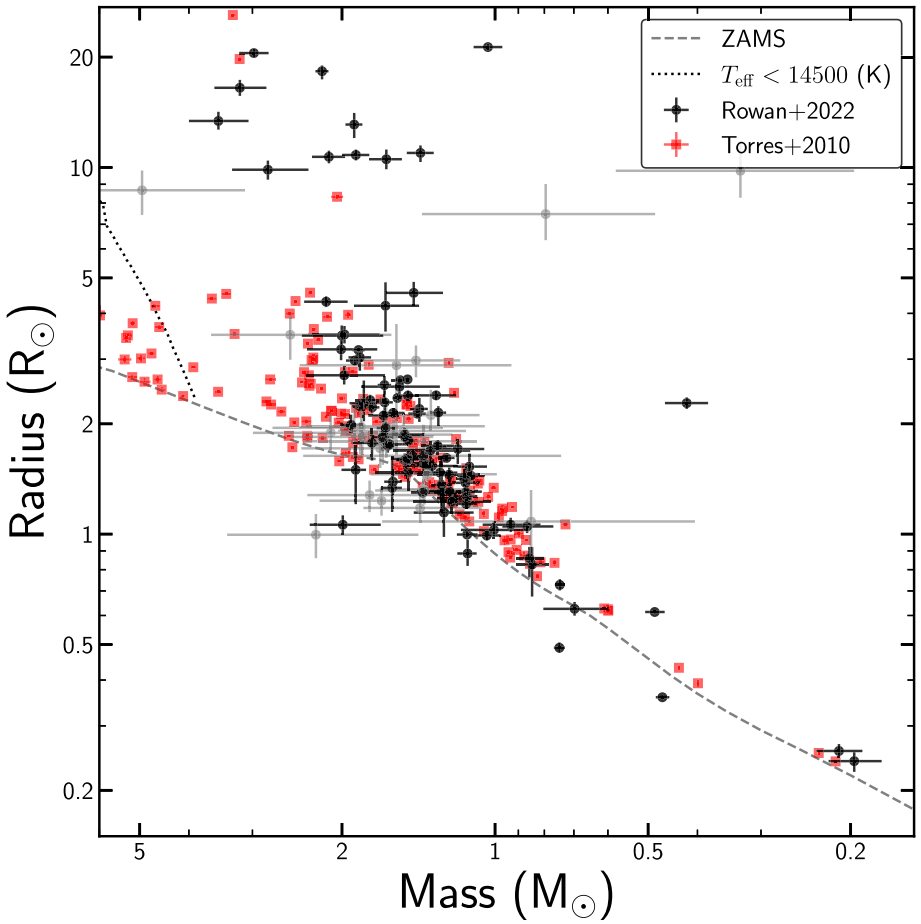

Figure 6. Masses and radii of eclipsing SB2s derived from ASAS-SN eclipsing binary light curves and *Gaia* SB2 orbital solutions. The grey points show stars with fractional mass error > 20 per cent. The Torres et al. (2010) catalogue stars are shown in red. The grey dashed line shows the MIST single-star ZAMS isochrone and the grey dotted line shows the cut-off at $T_{\rm eff} < 14\,500$ K for the *Gaia* RVS measurements.

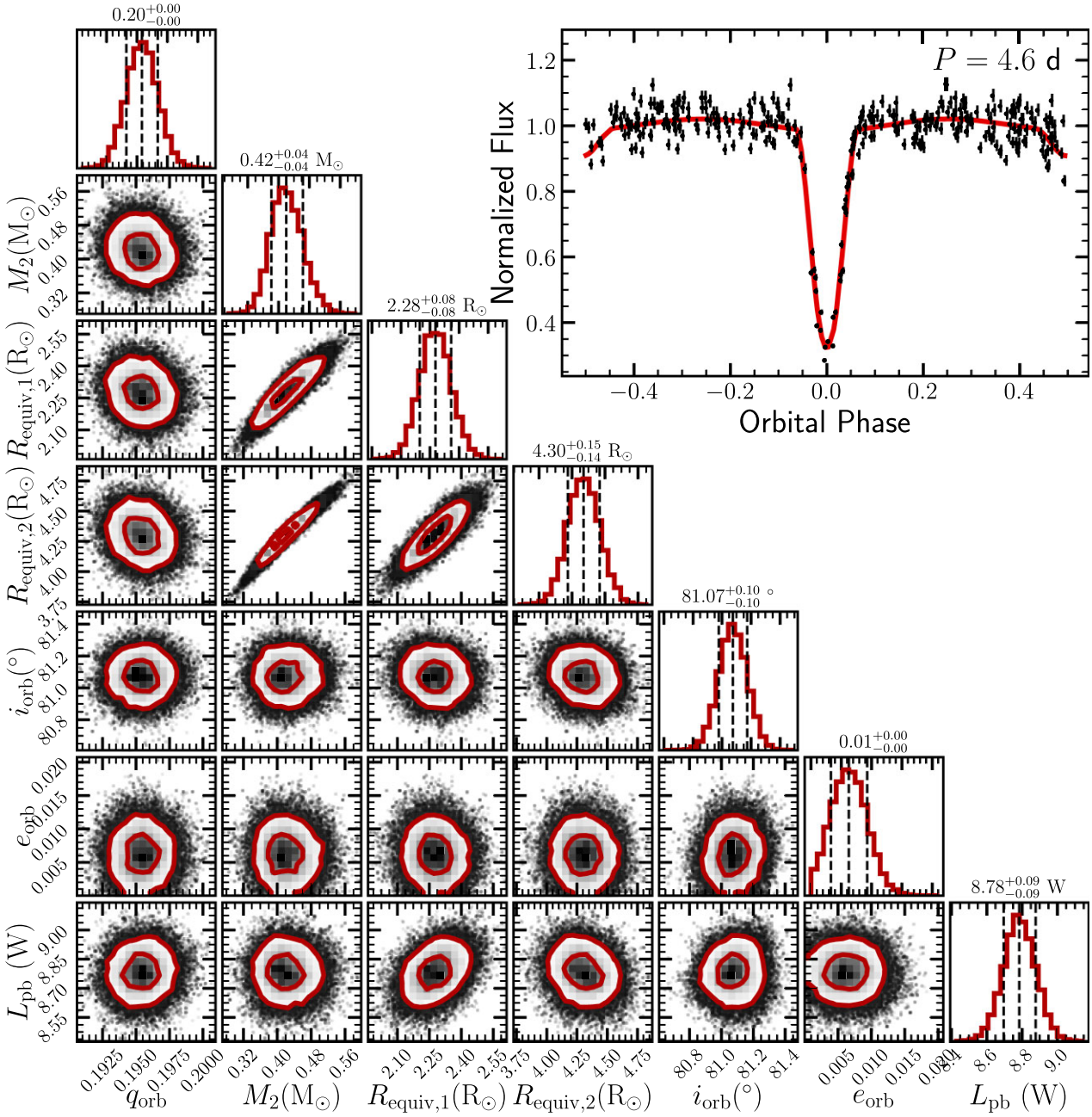

Figure 7. MCMC corner plot and light-curve fit for *Gaia* DR3 1762094209603752192. This binary has one star with $M < 1$ M$_\odot$ and $R > 2$ $R_\odot$ and one on the subgiant branch, which could suggest a history of mass transfer.

5 SUMMARY

Gaia Data Release 3 includes spectroscopic orbits for more than 181 000 SB1s and 5376 SB2s. We cross-match the catalogue of SB2s with our ASAS-SN eclipsing binary catalogue and further extend the sample through visual inspection. We compare the period and eccentricity from the ASAS-SN light curve to the *Gaia* values (Fig. 3) and find that only 50 per cent of systems have *Gaia* orbits in agreement with the light-curve fits. Although it is difficult to identify the source of the discrepancy in the *Gaia* solution without the individual RVs, we do see more disagreement at shorter periods and at fainter apparent magnitudes. For the single-lined binaries, Bashi et al. (2022) combined various *Gaia* radial velocity statistics to reject poor *Gaia* orbits and identified a sample of ∼90 000 of the ∼181 000 as having good SB1 orbits, but no such metrics currently exist for SB2s.

For the 70 systems where the *Gaia* solution is consistent with the eclipsing binary light curve, we use PHOEBE to fit the light curve constrained by the velocity semi-amplitudes to derive masses and radii for 122 stars. Of these 122 stars, 61 have fractional mass and radius uncertainties less than 10 per cent (Fig. 8). We find that many of the systems with high fractional mass errors use the *Gaia* circular orbit model 'SB2C', which tend to have larger uncertainties on K_2 (Fig. 9). The uncertainties in our catalogue are larger than those in the Torres et al. (2010) sample of eclipsing SB2s (Fig. 6), but we only use publicly available data from large surveys.

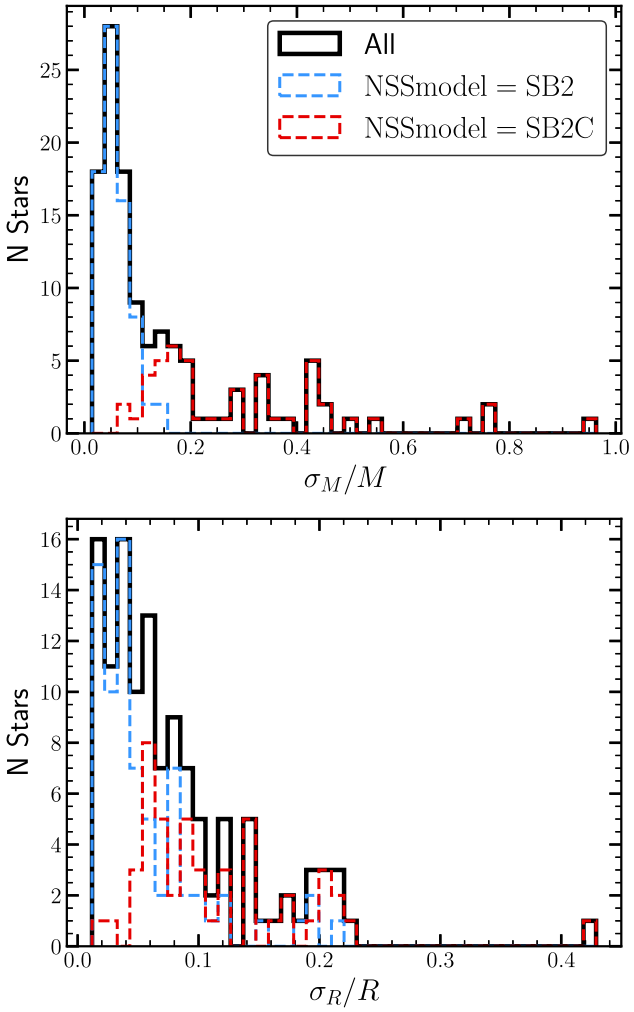

Figure 8. Fractional error on the masses (top) and radii (bottom) from the MCMC fits to the ASAS-SN light curves with orbital constraints from *Gaia* SB2s. The binaries with the circular orbital solution (NSSmodel = SB2C) make up the majority of the high fractional error tails in mass and radius.

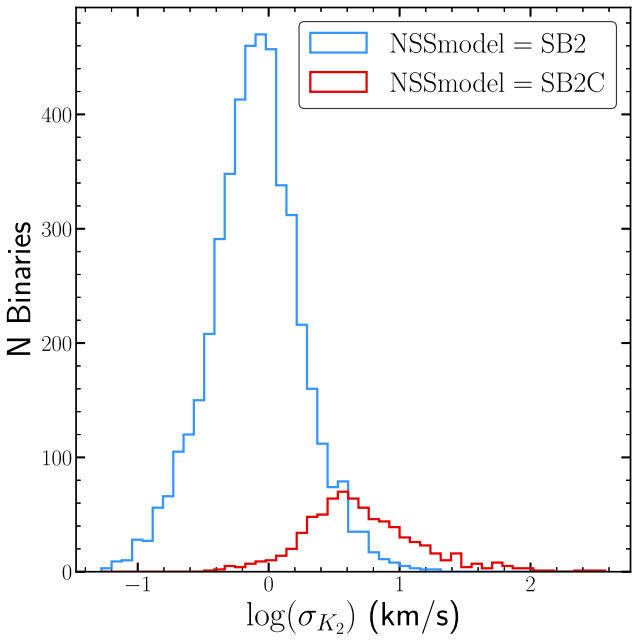

Figure 9. Distribution of the error on the velocity semi-amplitude of the secondary, σ_{K_2} for the full sample of *Gaia* SB2s coloured by the type of model used. The *Gaia* SB2s with the circular orbit model generally have larger errors on K_2.

Our sample is strongly limited by the differences between the magnitude range of ASAS-SN and the *Gaia* Radial Velocity Spectrometer. Since almost all of the *Gaia* SB2s are bright ($G < 12$ mag), and ASAS-SN light curves start to saturate at $G \sim 11$, only a fraction of the eclipsing spectroscopic binaries observed by *Gaia* have been modelled here. Large photometric surveys of brighter stars, such as ASAS (Pojmanski 2002; Paczyński et al. 2006) and the Kilodegree Extremely Little Telescope (Pepper et al. 2007) could be used to identify and characterize these brighter systems. The *Gaia* light curves often have too few epochs for modelling detached eclipsing binary light curves, but future releases will provide additional G, G_{BP}, and G_{RP} observations for millions of binaries. Multiband light curves could also be used to constrain absolute temperatures of the stars, providing additional constraints on relations between stellar parameters.

In total, we report masses and radii for 12 giants. One of these systems, *Gaia* DR3 5094313323276920 32, has the longest period, $P = 401.7$ d, and the highest eccentricity, $e = 0.46$, of the binaries in our sample. Since masses of giants are difficult to determine through isochrone fitting, these systems are valuable for expanding the small sample size of giants with precise physical parameters. Long time period photometry is crucial to detecting and characterizing these systems. Our ASAS-SN eclipsing binary catalogue contains more than 600 eclipsing binaries on the giant branch that could be used to expand the population of giants with dynamical masses and radii.

The sample of spectroscopic binaries will continue to expand with future *Gaia* data releases and upcoming spectroscopic surveys such as Milky Way Mapper (Kollmeier et al. 2017). Large catalogues of eclipsing binaries can be used not only to identify eclipsing SB2s, but also to provide initial conditions for detailed modelling of the light curve and radial velocity data.

ACKNOWLEDGEMENTS

We thank the PHOEBE developers for their help in troubleshooting. The authors would like to thank the anonymous reviewer for their comments that have improved the clarity of this paper. We thank Las Cumbres Observatory and its staff for their continued support of ASAS-SN. ASAS-SN is funded in part by the Gordon and Betty Moore Foundation through grants GBMF5490 and GBMF10501 to the Ohio State University, and also funded in part by the Alfred P. Sloan Foundation grant G-2021-14192.

DMR, KZS, and CSK were supported by NSF grant AST-1908570. Support for TJ was provided by NASA through the NASA Hubble Fellowship grant HF2-51509 awarded by the Space Telescope Science Institute, which is operated by the Association of Universities for Research in Astronomy, Inc., for NASA, under contract NAS5-26555.

This work has made use of data from the European Space Agency (ESA) mission *Gaia* (https://www.cosmos.esa.int/gaia), processed by the *Gaia* Data Processing and Analysis Consortium.

DATA AVAILABILITY

The ASAS-SN photometric data underlying this article are available in the ASAS-SN eclipsing binaries data base (https://asas-sn.osu.edu/binaries/mass-radius) and the ASAS-SN Photometry Database (https://asas-sn.osu.edu/photometry). The data underlying this article are available in the article and in its online supplementary material.

REFERENCES

Andersen J., 1991, A&AR, 3, 91
Bailer-Jones C. A. L., Rybizki J., Fouesneau M., Demleitner M., Andrae R., 2021, AJ, 161, 147
Bashi D., Shahaf S., Mazeh T., Faigler S., Dong S., El-Badry K., Rix H. W., Jorissen A., 2022, MNRAS, 517, 3888
Beck P. G. et al., 2014, A&A, 564, A36
Beck P. G. et al., 2022, A&A, 667, A31
Benbakoura M. et al., 2021, A&A, 648, A113
Bhatti W., lgbouma J., 2018, Waqasbhatti/Astrobase: Astrobase V0.3.8
Bódi A., Hajdu T., 2021, ApJS, 255, 1
Bovy J., Rix H.-W., Green G. M., Schlafly E. F., Finkbeiner D. P., 2016, ApJ, 818, 130
Brogaard K. et al., 2018, MNRAS, 476, 3729
Choi J., Dotter A., Conroy C., Cantiello M., Paxton B., Johnson B. D., 2016, ApJ, 823, 102
Conroy K. E. et al., 2020, ApJS, 250, 34
Cui X.-Q. et al., 2012, Res. Astron. Astrophys., 12, 1197
Dotter A., 2016, ApJS, 222, 8
Drimmel R., Cabrera-Lavers A., López-Corredoira M., 2003, A&A, 409, 205
Duck A., Gaudi B. S., Eastman J. D., Rodriguez J. E., 2022, preprint (arXiv:2209.09266)
Eastman J., Gaudi B. S., Agol E., 2013, PASP, 125, 83
Eggleton P. P., 1983, ApJ, 268, 368
Enoch B., Collier Cameron A., Parley N. R., Hebb L., 2010, A&A, 516, A33
Foreman-Mackey D., Hogg D. W., Lang D., Goodman J., 2013, PASP, 125, 306
Frandsen S. et al., 2013, A&A, 556, A138
Gaia Collaboration, 2022, preprint (arXiv:2208.00211)
Gao F., Han L., 2012, Optim. Appl., 51, 259
Gaulme P., McKeever J., Rawls M. L., Jackiewicz J., Mosser B., Guzik J. A., 2013, ApJ, 767, 82
Gaulme P., Jackiewicz J., Appourchaux T., Mosser B., 2014, ApJ, 785, 5
Gaulme P. et al., 2016, ApJ, 832, 121
Graczyk D. et al., 2011, AcA, 61, 103
Green G. M., Schlafly E., Zucker C., Speagle J. S., Finkbeiner D., 2019, ApJ, 887, 93
Hambleton K., Prša A., Fleming S. W., Mahadevan S., Bender C. F., 2022, ApJ, 931, 75
Hart K. et al., 2023, preprint (arXiv:2304.03791)
Hekker S. et al., 2010, ApJ, 713, L187
Hełminiak K. G. et al., 2021, MNRAS, 508, 5687
Huang C. X. et al., 2020a, Res. Notes Am. Astron. Soc., 4, 204
Huang C. X. et al., 2020b, Res. Notes Am. Astron. Soc., 4, 206
Jayasinghe T. et al., 2019, MNRAS, 486, 1907
Jayasinghe T., Rowan D. M., Thompson T. A., Kochanek C. S., Stanek K. Z., 2023, MNRAS, 521, 5927
Kirk B. et al., 2016, AJ, 151, 68
Kjeldsen H., Bedding T. R., 1995, A&A, 293, 87
Kochanek C. S. et al., 2017, PASP, 129, 104502
Kollmeier J. A. et al., 2017, preprint (arXiv:1711.03234)
Kounkel M. et al., 2021, AJ, 162, 184
Kovács G., Zucker S., Mazeh T., 2002, A&A, 391, 369
Kunimoto M. et al., 2021, Res. Notes Am. Astron. Soc., 5, 234
Majewski S. R. et al., 2017, AJ, 154, 94
Marshall D. J., Robin A. C., Reylé C., Schultheis M., Picaud S., 2006, A&A, 453, 635
Mowlavi N. et al., 2017, A&A, 606, A92
Orosz J. A., Hauschildt P. H., 2000, A&A, 364, 265
Paczyński B., Szczygieł D. M., Pilecki B., Pojmański G., 2006, MNRAS, 368, 1311
Pawlak M. et al., 2013, Acta Astron., 63, 323
Pepper J. et al., 2007, PASP, 119, 923
Petrosky E., Hwang H.-C., Zakamska N. L., Chandra V., Hill M. J., 2021, MNRAS, 503, 3975
Pietrukowicz P. et al., 2013, Acta Astron., 63, 115
Pojmanski G., 2002, Acta Astron., 52, 397
Pourbaix D. et al., 2004, A&A, 424, 727
Prša A., Zwitter T., 2005, ApJ, 628, 426
Prša A., Guinan E. F., Devinney E. J., DeGeorge M., Bradstreet D. H., Giammarco J. M., Alcock C. R., Engle S. G., 2008, ApJ, 687, 542
Prša A. et al., 2011, AJ, 141, 83
Prša A. et al., 2016, ApJS, 227, 29
Prša A. et al., 2022, ApJS, 258, 16
Qian S.-B., He J.-J., Zhang J., Zhu L.-Y., Shi X.-D., Zhao E.-G., Zhou X., 2017, Res. Astron. Astrophys., 17, 087
Qian S. B., Zhang J., He J. J., Zhu L. Y., Zhao E. G., Shi X. D., Zhou X., Han Z. T., 2018, ApJS, 235, 5
Ratajczak M. et al., 2021, MNRAS, 500, 4972
Ricker G. R. et al., 2015, J. Astron. Telesc. Instrum. Syst., 1, 014003
Rodríguez Martínez R. et al., 2023, AJ, 165, 97
Rowan D. M. et al., 2022, MNRAS, 517, 2190
Rowan D. M. et al., 2023, MNRAS, 520, 2386
Shappee B. J. et al., 2014, ApJ, 788, 48
Slawson R. W. et al., 2011, AJ, 142, 160
Soszyński I. et al., 2016, Acta Astron., 66, 405
Steinmetz M. et al., 2006, AJ, 132, 1645
Themeßl N. et al., 2018, MNRAS, 478, 4669
Torres G., Andersen J., Giménez A., 2010, A&AR, 18, 67

SUPPORTING INFORMATION

Supplementary data are available at *MNRAS* online.

Table 1. Stellar parameters from the MCMC fits to the ASAS-SN light curves with constraints from *Gaia* spectroscopic orbits.

Please note: Oxford University Press is not responsible for the content or functionality of any supporting materials supplied by the authors. Any queries (other than missing material) should be directed to the corresponding author for the article.

This paper has been typeset from a TEX/LATEX file prepared by the author.